Ab initio study on the size effect of symmetric and asymmetric ferroelectric tunnel junctions: A comprehensive picture...

Article *in* Journal of Applied Physics · August 2013

DOI: 10.1063/1.4817656

5 authors, including:

Yue Zheng
National University of Singapore
81 PUBLICATIONS **713** CITATIONS
SEE PROFILE

Xin Luo
National University of Singapore; Institute Of...
26 PUBLICATIONS **785** CITATIONS
SEE PROFILE

Biao Wang
Sun Yat-Sen University
121 PUBLICATIONS **1,399** CITATIONS
SEE PROFILE

Chung Ho Woo
City University of Hong Kong
239 PUBLICATIONS **3,948** CITATIONS
SEE PROFILE

AIP Journal of Applied Physics

Ab initio study on the size effect of symmetric and asymmetric ferroelectric tunnel junctions: A comprehensive picture with regard to the details of electrode/ferroelectric interfaces

W. J. Chen, Yue Zheng, X. Luo, B. Wang, and C. H. Woo

Citation: Journal of Applied Physics **114**, 064105 (2013); doi: 10.1063/1.4817656
View online: http://dx.doi.org/10.1063/1.4817656
View Table of Contents: http://scitation.aip.org/content/aip/journal/jap/114/6?ver=pdfcov
Published by the AIP Publishing

JOURNAL OF APPLIED PHYSICS **114**, 064105 (2013)

Ab initio study on the size effect of symmetric and asymmetric ferroelectric tunnel junctions: A comprehensive picture with regard to the details of electrode/ferroelectric interfaces

W. J. Chen,[1,2] Yue Zheng,[1,2,3,a)] X. Luo,[2,4] B. Wang,[1,2,b)] and C. H. Woo[3]
[1]*State Key Laboratory of Optoelectronic Materials and Technologies, School of Physics and Engineering, Sun Yat-sen University, 510275 Guangzhou, China*
[2]*Micro&Nano Physics and Mechanics Research Laboratory, School of Physics and Engineering, Sun Yat-sen University, 510275 Guangzhou, China*
[3]*Department of Physics and Materials, City University of Hong Kong, Kowloon, Hong Kong, China*
[4]*Institute of High Performance Computing, 1 Fusionopolis Way, #16-16 Connexis, Singapore 138632, Singapore*

(Received 26 June 2013; accepted 22 July 2013; published online 9 August 2013)

Ferroelectric size effect of $BaTiO_3$ (BTO) tunnel junctions with metal Pt and/or oxide $SrRuO_3$ (SRO) electrodes has been comprehensively investigated by the first-principle calculations. A vacuum layer is included in the supercell calculations, so that full-relaxation is achieved without artificial constraint on the supercell strains. We have constructed all of ten possible types of tunnel junctions with either symmetric or asymmetric geometries to systematically explore the influence of electrode/ferroelectric interfaces. The characteristics of atomic structure, polarization, charge density, and electrostatic potential for different geometries and sizes are revealed. It is found that the ferroelectric stability of a tunnel junction depends significantly on the details of the two electrode/ferroelectric interfaces, which present specific short- and long-range properties, e.g., local bonding environment, electronic screening, built-in field, etc. Result shows that Pt/BTO interfaces have strong coupling with ferroelectric distortion and thus play more dominant roles than the SRO/BTO interfaces in affecting the ferroelectric stability of the tunnel junctions. Particularly, it is found that Pt_2/TiO_2 interface can induce collective ferroelectric distortion in the initially non-distorted barrier. With a full-relaxation of the strains, an abnormal enhancement of ferroelectricity by Pt_2/BaO interface due to Pt-O bonding effect is demonstrated, where a strong interfacial-bonding-related polarizing field is verified. Also importantly, polarization stability of asymmetric tunnel junctions is found dependent on direction, manifested with the appearing of a new critical thickness, below which the tunnel junction loses polarization bistability. Furthermore, it shows that the local features of a specific electrode/ferroelectric interface (e.g., the interfacial atomic structure, local polarization, charge transfer, and potential step) are well kept in different types of tunnel junctions. By analyzing and summarizing the results, our results suggest that traditional phenomenological models need several modifications in order to quantitatively reproduce the size effect of ferroelectric tunnel junctions. Our study provides a comprehensive picture of the ferroelectric size effect in BTO tunnel junctions as a function of electrode/ferroelectric interfaces and should have valuable implications for future studies and applications. [http://dx.doi.org/10.1063/1.4817656]

I. INTRODUCTION

Ferroelectrics have been under intensive research for many decades for their important roles in the field of advanced materials and technologies.[1–3] Driven by the need of device miniaturization and integration, in recent years increasing attentions are being paid to ferroelectric nanostructures (FNs) (see, e.g., reviewed papers[4–9]), including nanoscale ferroelectric thin films (FTFs), nanowires, nanotubes, nanodisks, nanodots, heterostructures, etc. Compared with those of the bulk counterparts, properties of FNs show sensitivity to size, interface, and boundary conditions.[10–17] In particular, due to the collective nature of ferroelectricity and its interplay with surface/interface, ferroelectric size effect of FNs should be strong and complicated. For a long time, it has been commonly accepted that ferroelectric size effect of FNs is dominated by the depolarization field caused by uncompensated or partially compensated bound charges,[18–20] which depresses the ferroelectricity and leads to large ferroelectric critical size. However, recent studies have shown that the details of electromechanical environments at surface/interface (e.g., interfacial bonding, screening, surface strains and adsorbates) are important in determining the overall ferroelectric size effect of FNs.[21–42] Mechanisms of ferroelectric enhancement, depression, or forming novel polarization patterns[17,21] in FNs are all possible. It is thus senseless to discuss the ferroelectric size effect of FNs without regard to the details of surface/interface.

With the progresses in calculation methods and experimental techniques, recent studies found that ferroelectricity can be retained in FTFs of several unit-cells thick,[25–42]

[a)] Electronic address: zhengy35@mail.sysu.edu.cn.
[b)] Electronic address: wangbiao@mail.sysu.edu.cn.

sparking a huge interest in exploring FTFs in the applications of nanoscale electronic devices, such as nanoscale ferroelectric capacitors and ferroelectric tunnel junctions (FTJs). In experiment, using a combination of electric force microscopy and piezoelectric microscopy, Tybell *et al.*[25] have found a stable polarization in a 4-nm thick epitaxial PZT film on $SrTiO_3$ (STO) substrate at room temperature. Fong *et al.*[26,27] adopted X-ray scattering and observed ferroelectric properties in epitaxial $PbTiO_3$ (PTO) films down to 1.2 nm. Using variable-temperature ultraviolet Raman spectroscopy, Tenne *et al.*[28] found that one-unit-cell-thick $BaTiO_3$ (BTO) layers in BTO/STO superlattices are ferroelectric. Subsequently, they showed the ferroelectric critical thickness (FCT) of strained BTO films grown on the STO substrate was about 1.6 nm.[29] Theoretically, a large amount of first-principle calculations have been performed to investigate the ferroelectric stability of FTFs.[30–32,34–40] Particularly, Junquera and Ghosez[30] predicted that the FCT of single domain BTO films between $SrRuO_3$ (SRO) electrodes is about 2.4 nm based on the so-called frozen-phonon method. For the same structure, with considering the relaxation of atoms at the interfaces, Gerra *et al.*[34] found that the FCT is further reduced to about 1.2 nm. Using a fixed-D method, Stengel *et al.* showed that the stability of ferroelectricity is not only affected by the electronic screening properties at the interface but also depends crucially on the interfacial chemical bonding, which can lead to an abnormal enhancement of ferroelectricity.[36] More recently, Rappe *et al.*[37] demonstrated that breaking in-plane symmetry of PTO/Pt interface can strengthen the electrode-oxide bonds and stabilize polarization with no critical-size limit. Moreover, based on first-principles calculations, modified phenomenological models have been proposed to quantitatively describe the short-range and long-range contributions of surface/interface to the ferroelectric size effect in FTFs.[35,37,38,41,42]

As a typical example of applications utilizing FTFs, FTJs with electrode/FTF/electrode geometry have been designed to show interesting polarization-related electronic transport properties.[16,43–48] While these properties make FTJs as promising basic elements in developing nanoscale-transducers, ultrahigh-density nonvolatile random-access memories, and other novel functional devices, the existence of FCT in FTJs can impose stringent limitations on these wonderful possibilities. On the one hand, to influence the tunneling resistance across the barrier by polarization change, polarization stability in the FTF barrier is very crucial. On the other hand, tunneling can only notably happen in barriers with thickness smaller than several nanometers. It is thus necessary to make the FCT of FTF barrier even smaller. In other words, FTJs only works well in a narrow range of thickness, with an upper bound being the tunneling critical thickness and a lower bound being the FCT. Owning to this reason, understanding the ferroelectric size effect and improving the ferroelectric stability of FTJs are the important issues of theoretical and experimental studies.

One worth noting in recent studies of FTJs is the increasing attentions paid to those with asymmetric geometries,[16,37–40,42–46] aiming to find additional asymmetry-related functionalities. Compared with symmetric FTJs (S-FTJs), asymmetric FTJs (A-FTJs) have different top and bottom electrodes or electrode/FTF interfaces. Consequently, the degeneracy of polarization states with anti-directions is broken in A-FTJs, leading to distinct size dependences of the two states. Furthermore, the properties of A-FTJs described by a scalar quantity (e.g., potential and conductance) should also have dependence on polarization direction. Indeed, making use of the inequivalent potential barrier with respect to polarization direction, Tsymbal *et al.*[16,43,44] have demonstrated in A-FTJs that orders of magnitude change of tunneling conductance can be obtained in response to polarization reversal in the barrier, namely giant electro-resistance (GER) effect. More recently, important features of A-FTJs, i.e., the built-in field, absence of the critical thickness for one polarization state and related effects like smearing of phase transition have been predicted.[16,38–40,42] These new features associated with A-FTJs should have important implications on the application and are all expected to be dependent on the details of electrode/FTF interfaces.

In literature, first-principle calculations have already been performed to reveal the ferroelectric size effect in BTO tunnel junctions.[16,30,31,34–36,38,40] Nevertheless, due to the different focus of these calculations, and the fact that various supercell models, approximations (e.g., local-density approximation vs. generalized-gradient approximation), and method details (e.g., frozen-phonon method vs. full relaxation method) were adopted among different groups, the existed results are difficult to compare at the quantitative level. A complete picture of the ferroelectric size effect in BTO tunnel junctions as a function of electrode/FTF interfaces is lacking. In this paper, we apply a systematic ab-initio density functional theory (DFT) investigation on the ferroelectric size effect of BTO tunnel junctions with metal Pt and/or oxide SRO electrodes. With comprehensively taking into account the details of electrode/FTF interfaces, the characteristics of atomic structure, polarization, charge density, and electrostatic potential for up to ten possible types of FTJs are revealed and discussed. Our study should have valuable implications for further studies and applications.

II. METHODOLOGY

The calculations are performed based on the DFT as implemented in Vienna ab initio Simulation Package (VASP).[49] A plane-wave basis set and projector augmented wave (PAW) potentials are employed.[50] The exchange-correlation potential is treated in the local density approximation (LDA).[51] The plane wave functions are expanded with the energy cutoff of 500 eV. To obtain the ground states of the FTJs, all the atoms are relaxed using a $8 \times 8 \times 1$ Monkhorst Pack grid for k-point sampling[52] until the Hellmann-Feynman force on each atom is less than 10 meV/Å.

In our simulations, the FTJs are modeled to be epitaxially grown on a thick STO (001) substrate. The simulation supercells are built up by aligning the (001) oriented BTO ferroelectric films with the Pt (001) and SRO (001) electrodes. The in-plane lattice constant of the supercells is constrained to be the theoretical lattice constant of cubic STO (3.8668 Å).[40] Relaxation of bulk Pt, SRO, and BTO lattices are performed under this constraint. The resulting tetragonal unit cells (without ferroelectric distortion) are then used as the building blocks for the supercells. We include a vacuum region of ∼20 Å in the supercell to separate the top and bottom electrodes of the perovskite films, so that full-relaxations are achieved without artificial constraint on the supercell strains. It was demonstrated recently by Kolpak *et al.*[53] that the isolated-capacitor model can give equivalent electrical short-circuit conditions with the superlattice model. For certainty, we have also checked some of the relaxation results by cutting off the vacuum region and re-relax the relaxed structure and found that the change in the atomic displacements is negligible.

To systematically explore the influence of electrode/ferroelectric interfaces, all of ten possible types of FTJ geometries are constructed completely. They include the symmetric ones, i.e., Pt/(TiO_2-BaO)$_m$-TiO_2/Pt, Pt/BaO-(TiO_2-BaO)$_m$/Pt, SRO/(TiO_2-BaO)$_m$-TiO_2/SRO and SRO/BaO-(TiO_2-BaO)$_m$/SRO, and the asymmetric ones, i.e., Pt/(TiO_2-BaO)$_m$/Pt, SRO/(TiO_2-BaO)$_m$/SRO, Pt/(TiO_2-BaO)$_m$-TiO_2/SRO, Pt/BaO-(TiO_2-BaO)$_m$/SRO, Pt/(TiO_2-BaO)$_m$/SRO, and Pt/(BaO-TiO_2)$_m$/SRO, with the number of perovskite unit-cells *m* ranging from 2 to 8 or 9 for each type of tunnel junctions. To eliminate the effect of the electrode thickness on the relevant properties of the system, at least seven monolayers are included in the Pt and SRO electrodes. With the investigation on these ten types of FTJs, the effects of four types of interfaces, i.e., Pt_2/TiO_2, Pt_2/BaO, RuO_2/BaO, and SrO/TiO_2, and of their combinations can be comprehensively presented. Fig. 1 depicts the schematic atomic structures of typical S-FTJs, A-FTJs, and the four types of interfaces. Note that for the Pt_2/TiO_2 and Pt_2/BaO interfaces, we only consider bonding configurations with the lowest energy,[31] i.e., with Pt atoms situated above the oxygen atoms on the TiO_2 terminated surface and above Ba and O atoms on the BaO terminated surface.

As the constructed supercells are initially without ferroelectric distortion, to explore the ferroelectric stability of the FTJs, the barrier region of the supercells is distorted by an out of plane ferroelectric distortion obtained from the bulk strained BTO before a full relaxation of the structures. For S-FTJs, we also keep the mirror symmetry of the initial structures (i.e., without ferroelectric distortion) and relax them into centrosymmetric state so as to have an insight into the interfacial effect in the absence of bulk ferroelectricity. For A-FTJs, both of positive and negative ferroelectric distortions are imposed to reveal the direction dependence of polarization stability. In following simulations, if not mentioned otherwise, the tunnel junctions are imagined to be horizontally placed as indicated by their formula. The direction from left to right (which is also the *z* direction) is then defined as positive. As an example, for tunnel junctions in formula Pt/(BaO-TiO_2)$_m$/SRO, the positive direction points from the left Pt_2/BaO interface to the right TiO_2/SrO interface. To be clear, we denote symbols "$P_0\rightarrow$" and "$P_0\leftarrow$" to indicate that the tunnel junction is *initially* with positive and negative ferroelectric distortion, respectively. Moreover, symbols "$P\rightarrow$" and "$P\leftarrow$" are also introduced to, respectively, represent the positive and negative polarization state of the *relaxed* tunnel junction. We calculate the local polarization within the BTO unit-cells using the Berry phase method[54] by evaluating $P = (e/V_{\text{unitcell}})\sum_i Z_i U_i$, where e is the electronic charge, V_{unitcell} is the volume of unit-cell, Z_i is the Born effective charge of the *i*th ion, and U_i is the displacement of the *i*th ion from its position in the bulk paraelectric state.

III. RESULTS AND DISCUSSION

A. Symmetric ferroelectric tunnel junctions (S-FTJs)

We first perform calculations on S-FTJs without an initial ferroelectric distortion, which can provide us an insight into the interfacial effect in the absence of bulk ferroelectricity due to the constraint of mirror symmetry. The calculated Ti-O rumpling of [001] TiO_2 monolayers (i.e., the relative displacement between Ti and O layers) and Ba-O rumpling

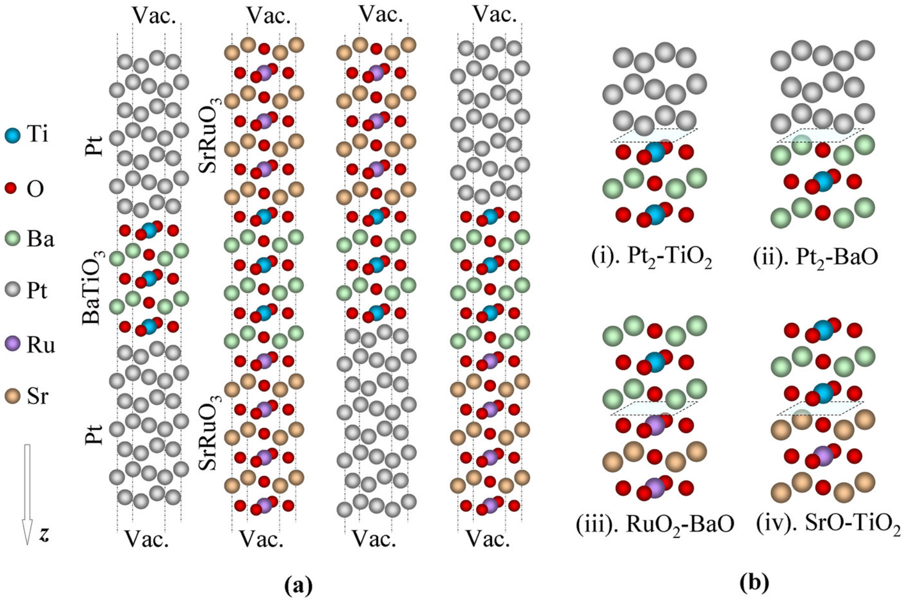

FIG. 1. (a) Schematic atomic structures of typical symmetric or asymmetric FTJs in our investigation. From left to right is Pt/(TiO_2-BaO)$_2$-TiO_2/Pt, SRO/(TiO_2-BaO)$_3$/SRO, Pt/(TiO_2-BaO)$_2$-TiO_2/SRO, and Pt/(TiO_2-BaO)$_3$/SRO tunnel junction. A vacuum region is included in the supercell to separate the top and bottom electrodes. (b) Four types of interfaces, i.e., (i) Pt_2/TiO_2 interface, (ii) Pt_2/BaO interface, (iii) RuO_2/BaO interface, and (iv) SrO/TiO_2 interface.

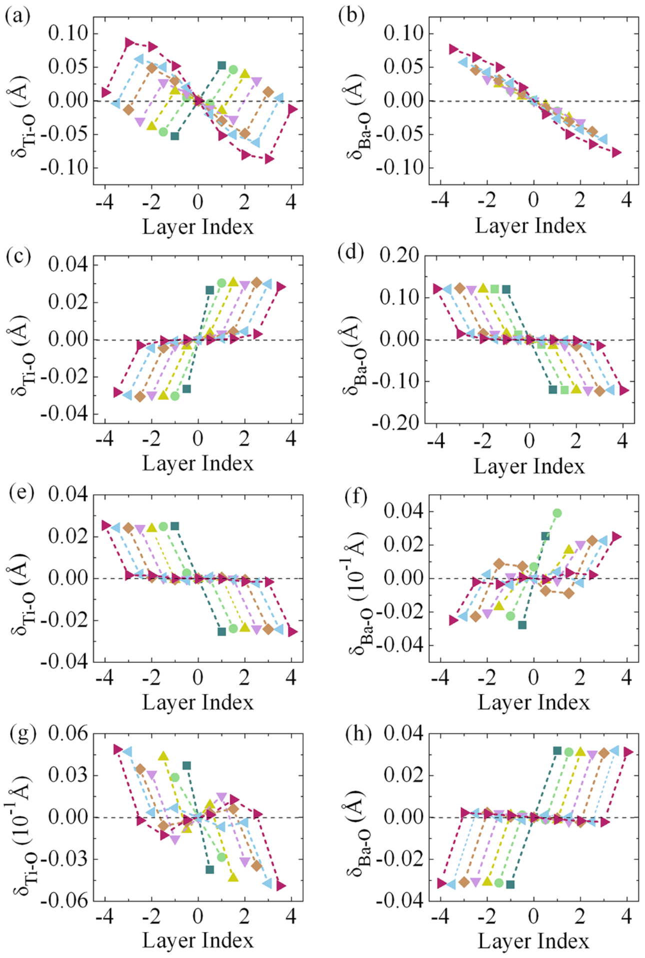

FIG. 2. Distribution of Ti-O rumpling of [001] TiO_2 monolayers (left column) and Ba-O rumpling of [001] BaO monolayers (right column) of the relaxed S-FTJs without an initial ferroelectric distortion. (a)–(b), (c)–(d), (e)–(f), and (h)–(g) are the results of Pt/$(TiO_2–BaO)_m$-TiO_2/Pt, Pt/BaO-$(TiO_2$-$BaO)_m$/Pt, SRO/$(TiO_2$-$BaO)_m$-TiO_2/SRO, and SRO/BaO-$(TiO_2$-$BaO)_m$/SRO tunnel junctions, respectively. The layer index is set zero at the middle plane of the barrier.

of [001] BaO monolayers in the relaxed S-FTJs are, respectively, depicted in the left and right column of Fig. 2. To be specific, Figs. 2(a)–2(b), 2(c)–2(d), 2(e)–2(f), and 2(g)–2(h) are the results of Pt/$(TiO_2$-$BaO)_m$-TiO_2/Pt, Pt/BaO-$(TiO_2$-$BaO)_m$/Pt, SRO/$(TiO_2$-$BaO)_m$-TiO_2/SRO, and SRO/BaO-$(TiO_2$-$BaO)_m$/SRO tunnel junctions, respectively, with *m* ranging from 2 to 8.

As can be seen from Fig. 2, due to the symmetry constraint during relaxation, the relaxed structures are all forced into centrosymmetric states. Nevertheless, the atomic rumplings of the four types of S-FTJs are found quite different, indicating strong dependence on the details of electrode/FTF interfaces. First, note that the atomic rumplings of tunnel junctions with Pt electrodes (Figs. 2(a)–2(d)) are generally more significant than those of tunnel junctions with SRO electrodes (Figs. 2(e)–2(f)). For example, a large Ba-O rumpling over 0.1 Å exists in the Pt_2/BaO interface of Pt/BaO-$(TiO_2$-$BaO)_m$/Pt tunnel junctions (Fig. 2(d)), which is much larger than that (∼0.03 Å) found at the RuO_2/BaO interface of SRO/BaO-$(TiO_2$-$BaO)_m$/SRO tunnel junctions (Fig. 2(h)). Second, Figs. 2(a)–2(b) show that the atomic rumpling profiles of Pt/$(TiO_2$-$BaO)_m$-TiO_2/Pt tunnel junctions exhibit both long-range and short-range features, whereas those of the latter three types of S-FTJs only exhibit short-range feature with large rumplings at the near-interfacial layers (Figs. 2(c)–2(h)). Furthermore, as clearly shown by the latter three types of S-FTJs, the magnitude of interfacial atomic rumplings keeps almost the same as the unit-cell number *m* changes, which implies that the short-range feature of the interface effect is size independent. Third, the Ti-O rumpling profiles are found in an opposite trend to the Ba-O rumpling profiles for each type of S-FTJs except Pt/$(TiO_2$-$BaO)_m$-TiO_2/Pt tunnel junctions.

Actually, for Pt/$(TiO_2$-$BaO)_m$-TiO_2/Pt tunnel junctions with large thickness (e.g., $m = 8$), two ferroelectric distorted regions with anti-directions are formed in the barrier, manifesting with a sine shape of Ti-O rumpling distribution and a linear shape of Ba-O rumpling distribution. This result is interesting as it implies that Pt_2/TiO_2 interface can induce a long-range ferroelectric distortion although the barrier is initially paraelectric and kept in mirror symmetry. Note that the induced long-range ferroelectric distortion points from the interface into the barrier. Meanwhile, the Pt_2/TiO_2 interface also induces short-range interfacial rumplings, with Ti-O (Ba-O) rumpling at the interface pointing to (away from) the electrode, similar with the result of Ref. 47. Due to this effect, the relaxed structures of Pt/$(TiO_2$-$BaO)_m$-TiO_2/Pt tunnel junctions with large *m* are centrosymmetric but not paraelectric. (In the following, nevertheless, we still call this state as paraelectric state.) Only for tunnel junction with two unit-cells, i.e., Pt/$(TiO_2$-$BaO)_2$-TiO_2/Pt, the long-rang effect is totally prohibited, and a real paraelectric state is formed.

The above result indicates that the Pt/BTO interfaces can induce more significant atomic rumplings in the barrier than the SRO/BTO interfaces, nevertheless, except for the Pt/$(TiO_2$-$BaO)_m$-TiO_2/Pt tunnel junctions, the coupling of the interface structure with the ferroelectric distortion is excluded. In the next, to further explore interfacial effects on the ferroelectric stability of S-FTJs, we relax the four types of S-FTJs with an initial positive ferroelectric distortion in the barrier (i.e., $P_0\!\rightarrow$ state). For example, a ferroelectric distortion from left Pt_2/TiO_2 to right TiO_2/Pt_2 interface is initially imposed to Pt/$(TiO_2$-$BaO)_m$-TiO_2/Pt tunnel junctions. Fig. 3 shows the calculated results for the four types of S-FTJs, where (a), (b), (c), and (d) labels the results of Pt/$(TiO_2$-$BaO)_m$-TiO_2/Pt, Pt/BaO-$(TiO_2$-$BaO)_m$/Pt, SRO/$(TiO_2$-$BaO)_m$-TiO_2/SRO, and SRO/BaO-$(TiO_2$-$BaO)_m$/SRO tunnel junctions, respectively, with *m* ranging from 2 to 8. Column from left to right depicts the Ti-O rumpling of [001] TiO_2 monolayers, the Ba-O rumpling of [001] BaO monolayers, the local polarization distribution, and the average polarization as a function of unit-cell number *m*, respectively.

For Pt/$(TiO_2$-$BaO)_m$-TiO_2/Pt tunnel junctions, as shown in the left panel of Fig. 3(a), it can be seen that the Ti-O rumpling distribution is inhomogeneous across the barrier. When the unit-cell number *m* of the barrier is above three, the Ti-O rumpling distribution is positive and asymmetric, indicating the appearance of net polarization across the barrier and a polarization-related asymmetric field. Otherwise, as *m* is smaller than three, the Ti-O rumpling distribution becomes

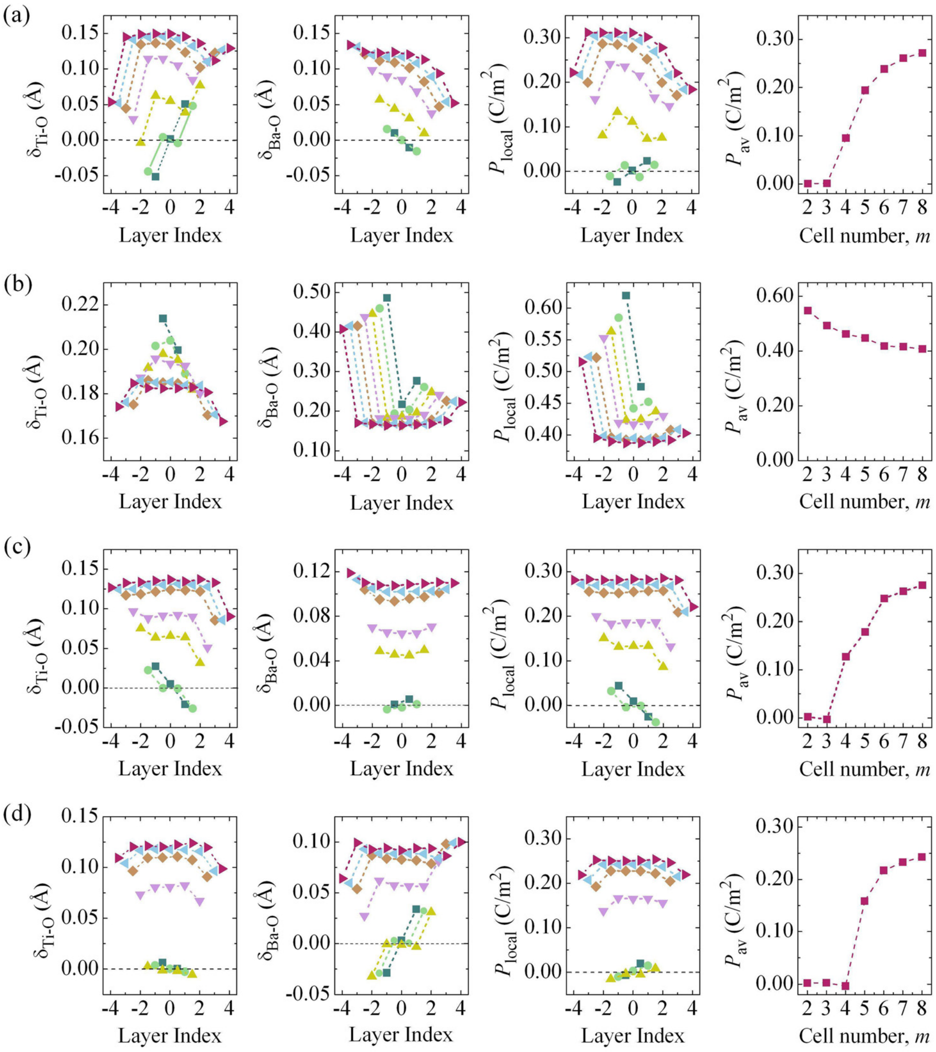

FIG. 3. Calculated atomic structure and polarization of the relaxed S-FTJs with an initial positive ferroelectric distortion. (a), (b), (c), and (d) labels are the results of Pt/$(TiO_2\text{-}BaO)_m$-TiO_2/Pt, Pt/BaO-$(TiO_2\text{-}BaO)_m$/Pt, SRO/$(TiO_2\text{-}BaO)_m$-TiO_2/SRO, and SRO/BaO-$(TiO_2\text{-}BaO)_m$/SRO, respectively. Column from left to right is the Ti-O rumpling of [001] TiO_2 monolayers, the Ba-O rumpling of [001] BaO monolayers, the local polarization distribution, and the average polarization as a function of unit-cell number m, respectively. The layer index is set zero at the middle plane of the barrier.

centrosymmetric and similar with that shown in Fig. 2(a), indicating the zero net polarization. Similar trend is found in the size dependence of the Ba-O rumpling as shown in the second panel of Fig. 3(a). Therefore, ferroelectric instability happens when the tunnel junction has less than four unit-cells. From the calculated local polarization and average polarization as shown in the last two panels of Fig. 3(a), the FCT of this type of tunnel junctions is indeed four unit-cells. As already pointed out (see Figs. 2(a)–2(b)), a combination of Pt/TiO_2 and TiO_2/Pt interfaces tends to induce a sine shape of Ti-O rumpling distribution and a linear shape of Ba-O rumpling distribution. These features are clearly reflected in the relaxation result of tunnel junctions with an initial ferroelectric distortion, demonstrating again the distinct coupling effect between the ferroelectric distortion and interfaces for this type of tunnel junctions.

The calculated results of Pt/BaO-$(TiO_2\text{-}BaO)_m$/Pt tunnel junctions with an initial positive ferroelectric distortion are depicted in Fig. 3(b). Compared with previous results of Pt/$(TiO_2\text{-}BaO)_m$-TiO_2/Pt tunnel junctions (see Fig. 3(a)), they show quite different features. From the first two panels of Fig. 3(b), we found that the atomic rumplings remain positive for all thickness and even increase in magnitude as the unit-cell number m decreases, indicating an abnormal enhancement of ferroelectricity. Particularly, for all thickness, a remarkable Ba-O rumpling over 0.4 Å is found at the left Pt_2/BaO interface. Compared this value with that (∼0.1 Å) of the tunnel junctions in centrosymmetric state (see Figs. 2(c)–2(d)), this remarkable Ba-O rumpling indicates a strong coupling of Pt_2/BaO interfacial structure with ferroelectric distortion. As will be seen in the following, Pt-O bonding plays an important role in this coupling. The inequivalent Pt-O bonding at the two interfaces induces a large polarizing field, which conversely assists the formation of bulk ferroelectricity. As shown in the last two panels of Fig. 3(b), FCT is absent in this type of tunnel junctions. There is a large local polarization at the left Pt_2/BaO interface, and the average polarization even increases as the unit-cell number m decreases. The possible effect of vacuum region has been checked by removing the vacuum region and re-relaxing the structures, and no significant difference is found. Furthermore, the energy of this ferroelectric state is found indeed smaller than the energy of the paraelectric state shown in Fig. 2(b). We think that a full relaxation of the strains of the tunnel junction is important to observe this abnormal ferroelectric size effect. This abnormal enhancement of ferroelectricity by the Pt/BaO interface was in accordance with the prediction by Stengel *et al.*,[36] who showed that the Pt-O bonding at the Pt_2/BaO interface can enhance ferroelectricity. We notice that the absence of critical-size in S-FTJs is also possible by breaking in-plane symmetry of metal/FTFs interfaces, which can strengthen the electrode-oxide bonds and stabilize polarization.[37]

As depicted in Figs. 3(c) and 3(d), the ferroelectric size effects of S-FTJs with SRO/BTO interfaces manifest themselves in a more conventional way compared with those of S-FTJs with Pt/BTO interfaces. For both types of S-FTJs, the calculated atomic rumplings and local polarization distributions are quite homogeneous within the barrier except at the interfacial regions, indicating the distinguishable long-range and short-range features of the interfaces. For SRO/$(TiO_2\text{-}BaO)_m$-TiO_2/SRO tunnel junctions with more than three unit-cells (see Fig. 3(c)), the atomic rumplings are positive and in asymmetric distribution, with the Ti-O rumpling having a much smaller magnitude at the right interface and the Ba-O rumpling having slightly larger magnitude at the interfacial regions. As the tunnel junction has three or less unit-cells, the atomic rumplings become centrosymmetric and near zero, indicating the instability of ferroelectric phase and a FCT about four unit-cells. Meanwhile, for SRO/BaO-$(TiO_2\text{-}BaO)_m$/SRO tunnel junctions (see Fig. 3(d)), it is found that the ferroelectric state is stable when the unit-cell number m is larger than four, i.e., critical thickness is five unit-cells. In the ferroelectric state of this type of tunnel junctions, the Ti-O rumpling has smaller magnitude at the interfacial regions, and a smaller (larger) Ba-O rumpling is found at the left (right) interfaces than the inner region. For both types of S-FTJs, the local polarization distribution of ferroelectric state is found in similar trend with the Ti-O rumpling. Notice that our calculated atomic rumpling patterns agree well with the reported ones by Tagantsev *et al.*;[35] however, the FCT of each type of tunnel junctions is one unit-cell larger than their reported value. This difference may be due to that we have used the local-density approximation rather than generalized-gradient approximation.

A series of computed structural parameters at different interfaces of S-FTJs with $m = 8$ are depicted in Table I. The parameters include the Pt-O bonding length at Pt_2/TiO_2 and Pt_2/BaO interfaces $L^z_{\text{Pt-O}}$, the Pt-Ba atomic distance at the Pt_2/BaO interface $L^z_{\text{Pt-Ba}}$, the Ti-O bonding length at the SrO/TiO_2 interface $L^z_{\text{Ti-O}}$, the Ru-O bonding length at the RuO_2/BaO interface $L^z_{\text{Ru-O}}$, and the atomic rumplings of [001] monolayers at the interfaces $\delta^{xy}_{\text{Ti-O}}$, $\delta^{xy}_{\text{Ba-O}}$, $\delta^{xy}_{\text{Sr-O}}$, and $\delta^{xy}_{\text{Ru-O}}$. With these parameters, the interfacial structures of the tunnel junctions can be fully characterized. To have a comprehensive insight into the coupling behavior between interfacial structure and polarization states of the tunnel junction, we list parameters at the left interface when the relaxed tunnel junction is in paraelectric state, positive polarization state ($P\rightarrow$), and negative polarization state ($P\leftarrow$).

From Table I, it can be seen that the interfacial structural parameters of a specific interface depend on the polarization state of the tunnel junction. The most notable dependence is found at those of Pt_2/BaO interface, especially the Pt-O bonding length, indicating its important role in determining the abnormal ferroelectric size effect of Pt/BaO-$(TiO_2\text{-}BaO)_m$/Pt tunnel junctions shown in Fig. 3(b). Specifically, as the tunnel junction is in paraelectric state, the Pt-O bonding length $L^z_{\text{Pt-O}}$, the Pt-Ba distance $L^z_{\text{Pt-Ba}}$, and the rumpling of interfacial BaO layer $\delta^{xy}_{\text{Ba-O}}$ is 2.286 Å, 2.869 Å, and 0.121 Å, respectively. When the tunnel junction is in $P\rightarrow$ ($P\leftarrow$) state, these three parameters change to be 2.062 Å (3.269 Å), 2.912 Å (3.136 Å), and 0.407 Å (−0.217 Å), respectively. From these parameters, it can be noted that the interfacial distance between the Pt layer and BaO layer changes a lot (∼1Å) when the polarization reverses. Besides, a significant rumpling of Pt layer $\delta^{xy}_{\text{Pt-Pt}}$ exists at the Pt_2/BaO interface, which is about 0.462 Å, 0.443 Å, and 0.084 Å for the three polarization states, respectively, by noticing that $\delta^{xy}_{\text{Pt-Pt}} = L^z_{\text{Pt-Ba}} - (L^z_{\text{Pt-O}} + \delta^{xy}_{\text{Ba-O}})$. One of the obtained parameter 0.462 Å rumpling of Pt layer in the centrosymmetric state is in good agreement with the one given by Stengel *et al.*[36] List of these parameters also show effect of interfaces on the ferroelectricity of FTJs.

For the other three types of interfaces, the structural parameters exhibit much less significant changes as the polarization state of the tunnel junction changes. For example, for Pt_2/TiO_2 interface, the Pt-O bonding length changes a little bit from 2.098 Å to 2.090 Å (2.132 Å) when the tunnel junction changes from the paraelectric state to $P\rightarrow$ ($P\leftarrow$) state. It is worth to note that a notable rumpling of the SrO layer $\delta^{xy}_{\text{Sr-O}}$ is observed at the SrO/TiO_2 interface when the tunnel junction is in ferroelectric state, which is in the same direction with the Ti-O rumpling, indicating a penetration of ferroelectric distortion into the SRO electrode. Contrarily, as shown by the rumpling of the RuO_2 layer $\delta^{xy}_{\text{Ru-O}}$, an interfacial Ru-O dipole directed from the electrode to the barrier is always found at RuO_2/BaO interface, irrespective with the ferroelectric state of the barrier.

To analyze the charge transfer of atomic bondings at the interfaces, we further investigated the differential electron charge density $\Delta\rho_{\text{scf-nscf}}$, which denotes the difference

TABLE I. Computed structural parameters (in unit Å) at the left interfaces of relaxed Pt/$(TiO_2\text{-}BaO)_8$-TiO_2/Pt, Pt/BaO-$(TiO_2\text{-}BaO)_8$/Pt, SRO/$(TiO_2\text{-}BaO)_8$-TiO_2/SRO, and SRO/BaO-$(TiO_2\text{-}BaO)_8$/SRO tunnel junctions. The tunnel junctions are in paraelectric, positive polarization ($P\rightarrow$), and negative polarization state ($P\leftarrow$).

	Pt_2-TiO_2		Pt_2-BaO			SrO-TiO_2			RuO_2-BaO		
States	$L^z_{\text{Pt-O}}$	$\delta^{xy}_{\text{Ti-O}}$	$L^z_{\text{Pt-O}}$	$L^z_{\text{Pt-Ba}}$	$\delta^{xy}_{\text{Ba-O}}$	$L^z_{\text{Ti-O}}$	$\delta^{xy}_{\text{Sr-O}}$	$\delta^{xy}_{\text{Ti-O}}$	$L^z_{\text{Ru-O}}$	$\delta^{xy}_{\text{Ru-O}}$	$\delta^{xy}_{\text{Ba-O}}$
paraelectric	2.098	0.012	2.286	2.869	0.121	1.913	0.011	0.025	2.013	0.093	−0.031
$P\rightarrow$	2.090	0.054	2.062	2.912	0.407	2.025	0.117	0.127	1.975	0.109	0.064
$P\leftarrow$	2.132	−0.126	3.269	3.136	−0.217	1.838	−0.092	−0.092	2.055	0.060	−0.107

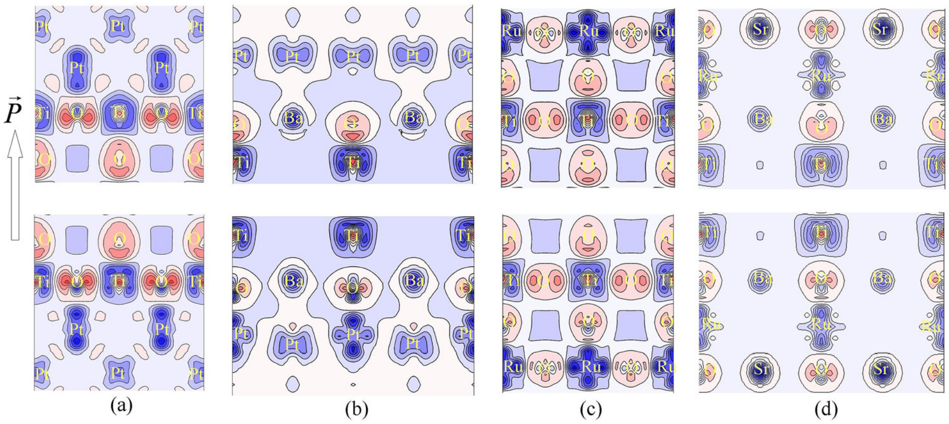

FIG. 4. Calculated differential charge density profile at the relaxed interfaces of (a) Pt/(TiO$_2$-BaO)$_8$-TiO$_2$/Pt, (b) Pt/BaO-(TiO$_2$-BaO)$_8$/Pt, (c) SRO/(TiO$_2$-BaO)$_8$-TiO$_2$/SRO, and (d) SRO/BaO-(TiO$_2$-BaO)$_8$/SRO tunnel junction. The tunnel junctions are in ferroelectric state with the direction of the polarization as indicated by the arrow. Electron loss is given by blue color and electron gain by red color.

between the self-consistent electron charge density and the non-self-consistent one (i.e., a superposition of atomic electron charge densities) of the relaxed supercell. Fig. 4 depicts $\Delta\rho_{\text{scf-nscf}}$ distribution (cut at the middle [100] or [110] plane of the supercell) at the interfaces of S-FTJs with $m=8$, which are relaxed into ferroelectric state with the polarization direction as indicted by the arrow. As oxygen atoms tend to gain electrons from the other atoms after bonding, for tunnel junctions with Pt electrodes, it is clearly seen that there is an electron loss (red color) at the electrodes and an electron gain (blue color) in the ferroelectric barrier (see Figs. 4(a)–4(b)). Actually, although not obvious from the Figs. 4(c)–4(d), similar trend of charge transfer happens in tunnel junctions with SRO electrodes. Moreover, result shows that the asymmetric interfacial structure at the left and right interfaces due to ferroelectric distortion can lead to dissimilar interfacial bonding environments and redistributes the interfacial charge density. Particularly as shown in Fig. 4(b), due to the strong coupling between Pt-O bonding and local ferroelectric distortion, the bonding environment and interfacial charge density are very different at the two interfaces. As can be expected, due to this asymmetric structure, electrostatic properties such as the screen ability, work function, and potential steps should be varied for the two interfaces.

To see the charge transfer at the interfaces of S-FTJs more clearly, in Fig. 5, we plot the macroscopic-averaged differential electron charge density along z direction $\Delta\bar{\bar{\rho}}_{\text{scf-nscf}}(z)$ for S-FTJs with $m=8$ using a double-macroscopic-average method.[55,56] For comparison, both paraelectric and ferroelectric states are presented. Consistent with Fig. 4, for all the tunnel junctions, there is an electron loss at the electrodes and an electron gain in the ferroelectric barrier. Particularly, the charge transfer is larger at the Pt/BTO interfaces than that at the SRO/BTO interfaces. Comparison between the curves of paraelectric and ferroelectric states shows that $\Delta\bar{\bar{\rho}}_{\text{scf-nscf}}(z)$ becomes asymmetric when the tunnel junction changes into ferroelectric state, indicating the appearance of polarization charge in the barrier surface and the screening charge in the electrodes. Interestingly, the difference in $\Delta\bar{\bar{\rho}}_{\text{scf-nscf}}(z)$ between the paraelectric and ferroelectric states is found more significant at the SRO/BTO interfaces (see Figs. 5(c)–5(d)) than at the Pt/BTO interfaces (see Figs. 5(a)–5(b)). This implies that the coupling between electron transfer and the ferroelectric distortion at the SRO/BTO interfaces is more sensitive than the Pt/BTO interfaces.

As can be expected, the distinct interfacial charge transfer and its coupling with ferroelectric distortion at various interfaces (see Figs. 4 and 5) should affect the potential distribution in the tunnel junction. This will further impose important effect on the electronic properties of the tunnel junction. The macroscopic-averaged electrostatic potential energy profile along z direction $\bar{\bar{V}}(z)$ for S-FTJs with $m=8$ in both paraelectric and ferroelectric states is depicted Fig. 6. It can be seen that the potential profiles converge to constant levels inside the electrodes. For tunnel junctions in their paraelectric state (except Pt/(TiO$_2$-BaO)$_8$-TiO$_2$/Pt tunnel junction), the profiles are also quite flat inside the barrier, indicating a convergence to the bulk level. Meanwhile, for Pt/(TiO$_2$-BaO)$_8$-TiO$_2$/Pt tunnel junction in paraelectric state as shown in Fig. 6(a), there is nonzero electric field distribution inside the barrier due to the appearance of anti-polarized regions. As a consequence of larger interfacial charge transfer between the Pt electrode and the barrier, Pt/BTO

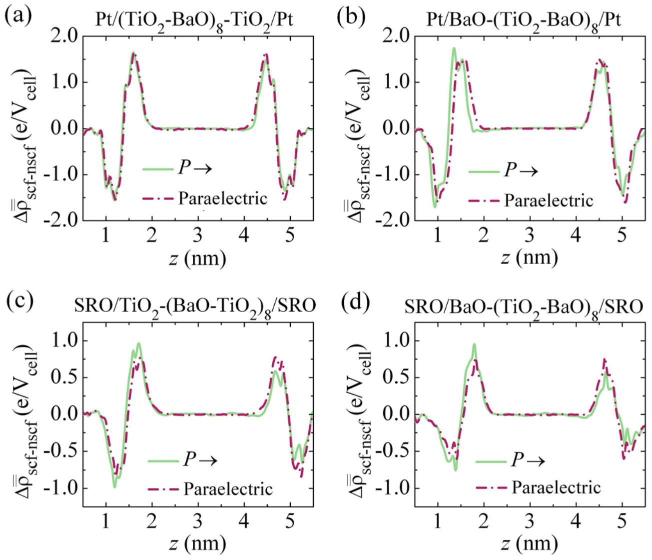

FIG. 5. Macroscopic-averaged differential charge density along z direction of S-FTJs in paraelectric and positive polarization states. e is the charge of an electron and V_{cell} is the volume of the supercell. (a) Pt/(TiO$_2$-BaO)$_8$-TiO$_2$/Pt, (b) Pt/BaO-(TiO$_2$-BaO)$_8$/Pt, (c) SRO/(TiO$_2$-BaO)$_8$-TiO$_2$/SRO, and (d) SRO/BaO-(TiO$_2$-BaO)$_8$/SRO tunnel junction.

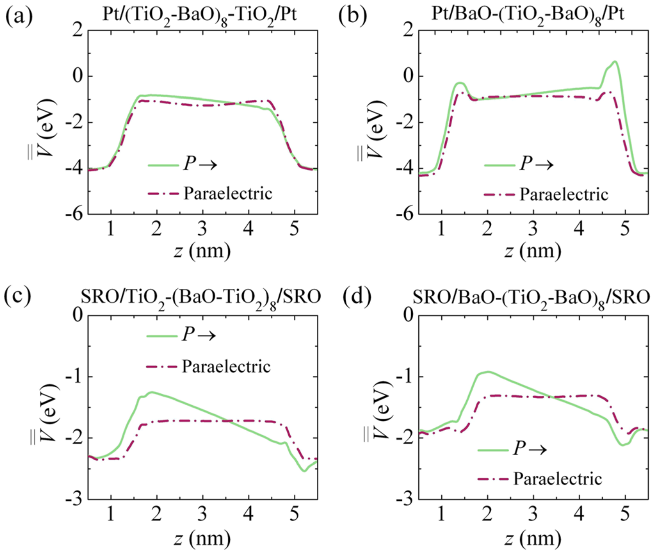

FIG. 6. Macroscopic-averaged electrostatic potential energy profile along z direction of S-FTJs in paraelectric and positive polarization states. (a) Pt/(TiO$_2$-BaO)$_8$-TiO$_2$/Pt, (b) Pt/BaO-(TiO$_2$-BaO)$_8$/Pt, (c) SRO/(TiO$_2$-BaO)$_8$-TiO$_2$/SRO, and (d) SRO/BaO-(TiO$_2$-BaO)$_8$/SRO tunnel junction.

interfaces have larger potential steps (i.e., the difference between the potential levels at the inner region of electrode and barrier) than SRO/BTO interfaces. According to the data of Pt/BaO-(TiO$_2$-BaO)$_8$/Pt and SRO/(TiO$_2$-BaO)$_8$-TiO$_2$/SRO tunnel junction as shown in Figs. 6(b) and 6(c), the difference is estimated to be ∼2.8 eV.

For tunnel junctions in ferroelectric states, due to the appearance of net polarization, non-centrosymmetric potential profiles are expected. Indeed, as shown in Fig. 6(a), a depolarizing field of about -2.0×10^8 V/m is found in the barrier of Pt/(TiO$_2$-BaO)$_8$-TiO$_2$/Pt tunnel junction in ferroelectric state. Meanwhile, Fig. 6(b) implies a large polarizing field of about 2.2×10^8 V/m in the ferroelectric state of Pt/BaO-(TiO$_2$-BaO)$_8$/Pt tunnel junction. For the SRO/(TiO$_2$-BaO)$_8$-TiO$_2$/SRO and SRO/BaO-(TiO$_2$-BaO)$_8$/SRO tunnel junctions (see Figs. 6(c) and 6(d)), the potential distributions are similar and the depolarization field is about -3.2×10^8 V/m and -3.0×10^8 V/m, respectively. Note that unlike the other three types of interfaces, there is a significant potential peak at the Pt$_2$/BaO interface, due to the large interfacial distance at this interface (see Table I). From the computed structural parameters in Table I, we can see that the large polarizing field originates from the inequal change of the potential steps at the two Pt/BTO interfaces. Moreover, it is worth to note that the average height of the potential barrier is slightly larger in the ferroelectric state for all tunnel junctions. This might indicate a larger electroresistance of the tunnel junction in the ferroelectric state than the paraelectric state.

B. Asymmetric ferroelectric tunnel junctions (A-FTJs)

Up to now, all the results presented are about S-FTJs. In realistic devices, the FTJs are likely in asymmetric geometries, which may bring distinct effects that are absent in S-FTJs. In the following, we focus on A-FTJs, including those with similar electrodes but different interfacial bondings, i.e., Pt/(TiO$_2$-BaO)$_m$/Pt and SRO/(BaO-TiO$_2$)$_m$/SRO, and those with dissimilar electrodes, i.e., Pt/(TiO$_2$-BaO)$_m$-TiO$_2$/SRO, Pt/BaO-(TiO$_2$-BaO)$_m$/SRO, Pt/(BaO-TiO$_2$)$_m$/SRO, and Pt/(TiO$_2$-BaO)$_m$/SRO, with the number of unit-cells m ranging from 2 to 8 or 9. Similar with the previous study on S-FTJs, we investigate the ferroelectric stability of the A-FTJs by relaxing the supercells with an initial ferroelectric distortion in the barrier region. Due to the asymmetry of these A-FTJs, the polarization states along the positive and negative directions are no longer equivalent. Therefore, both positive and negative ferroelectric distortions are initially imposed to the tunnel junction to reveal the direction dependence of polarization stability, with the two initial states denoted as "P_0→" and "P_0←."

To show the importance of interfacial bondings in affecting the ferroelectric size effect, we first investigate the A-FTJs with similar electrodes but different interfacial bondings. The calculated results of Pt/(TiO$_2$-BaO)$_m$/Pt tunnel junctions are shown in Fig. 7, including the atomic rumplings of [001] TiO$_2$ and BaO monolayers in the barrier, the local polarization and thickness dependence of the average polarization. Compared with the results of S-FTJs with Pt electrodes in the same polarization state (see Figs. 3(a)–3(b)), the atomic rumplings and local polarization near the specific interface (e.g., Pt$_2$/TiO$_2$ or Pt$_2$/BaO interfaces) are found similar, which reflects that the local feature of a specific interface is well kept in different types of tunnel junctions. For example, the significant depressing effect of left Pt$_2$/TiO$_2$ interface on the positive Ti-O rumpling can be clearly seen in Fig. 7. More importantly, despite the similar top and bottom electrodes, the positive and negative

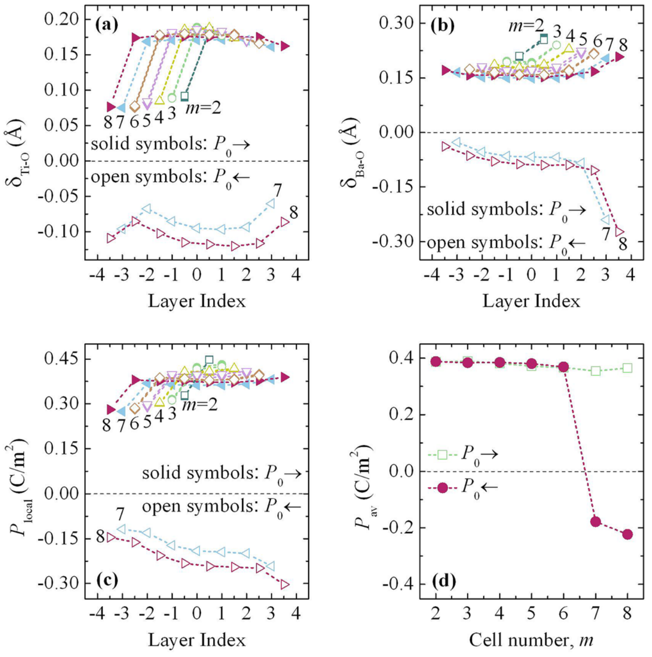

FIG. 7. Calculated results of Pt/(TiO$_2$-BaO)$_m$/Pt tunnel junctions with initial positive and negative ferroelectric distortions. (a) Ti-O rumpling of [001] TiO$_2$ monolayers. (b) Ba-O rumpling of [001] BaO monolayers. (c) Local polarization distribution. (d) Average polarization as a function of unit-cell number m. The layer index is set zero at the middle plane of the barrier.

polarization states are no longer equivalent due to the dissimilar interfacial bondings. Specifically, note that the rumplings for the two states (e.g., $m = 8$) are qualitatively different. Furthermore, the polarization stability exhibit dependence on direction. Specifically, for all thickness (i.e., m from 2 to 8), tunnel junctions with an initial positive ferroelectric distortion are relaxed into the positive polarization state. Meanwhile, for tunnel junctions with an initial negative ferroelectric distortion, only those with large thickness (i.e., $m = 7$, 8) are relaxed into the negative polarization state, with the others relaxed into the positive polarization state. In other words, there is no critical thickness for the positive polarization state and a large critical thickness about seven unit-cells for the negative polarization state. From the calculated polarization as depicted in Figs. 7(c)–7(d), we can also see that the polarization of positive state even increases a little bit as the barrier thickness decreases. Comparing with the result of Fig. 3(b), we consider that Pt_2/BaO interface plays an important role in this polarization enhancement.

For SRO/(BaO-TiO_2)$_m$/SRO tunnel junctions with m ranging from 2 to 8, the calculated results of the atomic rumplings of [001] monolayers, the local polarization and the average polarization as a function of thickness are shown in Fig. 8. Again, the atomic rumplings and local polarization near the specific interface (e.g., TiO_2/SrO or RuO_2/BaO interfaces) are found similar with those of the S-FTJs (see Figs. 3(c)–3(d)). Moreover, the polarization states along different directions are inequivalent with each other. Particularly, polarization state along the positive direction (i.e., from the RuO_2/BaO to TiO_2/SrO interface) is found more stable for this type of tunnel junctions, consistent with the work of Gerra *et al.*[38] For tunnel junctions with an initial negative ferroelectric distortion, those with less than six unit-cells will relax into a positive polarization state, indicating a loss of stability for the negative polarization state. Compared with the result of Pt/(TiO_2-BaO)$_m$/Pt tunnel junctions as shown in Fig. 7, the asymmetry of the SRO/(BaO-TiO_2)$_m$/SRO tunnel junctions is less significant, due to the similarity of TiO_2/SrO and RuO_2/BaO interfaces. Unlike the polarization enhancement found in Pt/(TiO_2-BaO)$_m$/Pt tunnel junctions, the polarization of SRO/(BaO-TiO_2)$_m$/SRO tunnel junctions continually deceases as the barrier thickness decreases and becomes zero when the unit-cell number m is two as shown in Figs. 8(c)–8(d). From this result, it can be seen that the more stable polarization state of A-FTJ is not necessary absence of critical thickness. Note also that at $m = 5$, the positive polarization state obtained in tunnel junctions with an initial negative ferroelectric distortion has smaller atomic rumplings and polarization magnitude than that obtained in tunnel junctions with an initial positive ferroelectric distortion. This indicates that the energy surface of the tunnel junction may have multiple valleys along a given direction of polarization.

As all the investigated FTJs so far are with similar top and bottom electrodes, it would be interesting to see whether adopting dissimilar top and bottom electrodes can brought new features, such as giant electro-resistance effect (GER),[16,43,44] giant piezoelectric resistance effect (GPR),[45,48] etc. The relaxation results of Pt/(TiO_2-BaO)$_m$-TiO_2/SRO tunnel junctions with initial positive and negative ferroelectric distortion are shown in Fig. 9. It can be seen that despite the dissimilar electrodes in the A-FTJs, the

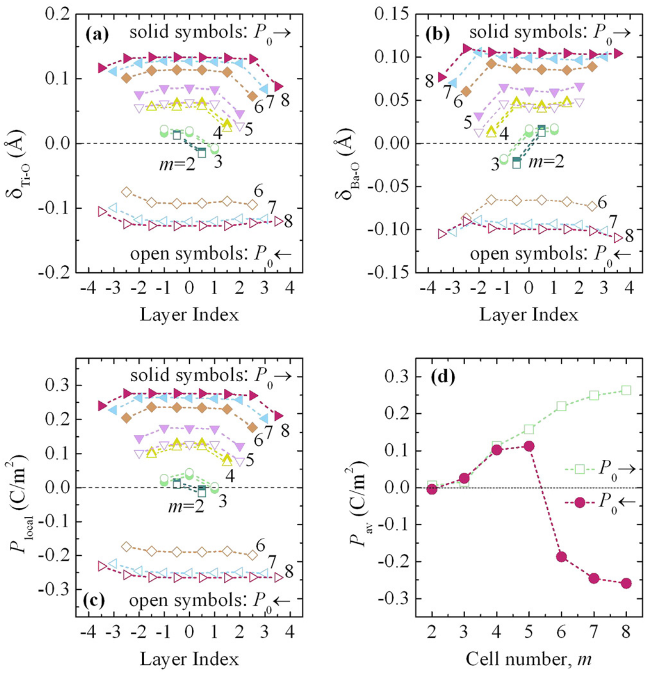

FIG. 8. Calculated results of SRO/(BaO-TiO_2)$_m$/SRO tunnel junctions with initial positive and negative ferroelectric distortions. (a) Ti-O rumpling of [001] TiO_2 monolayers. (b) Ba-O rumpling of [001] BaO monolayers. (c) Local polarization distribution. (d) Average polarization as a function of unit-cell number m. The layer index is set zero at the middle plane of the barrier.

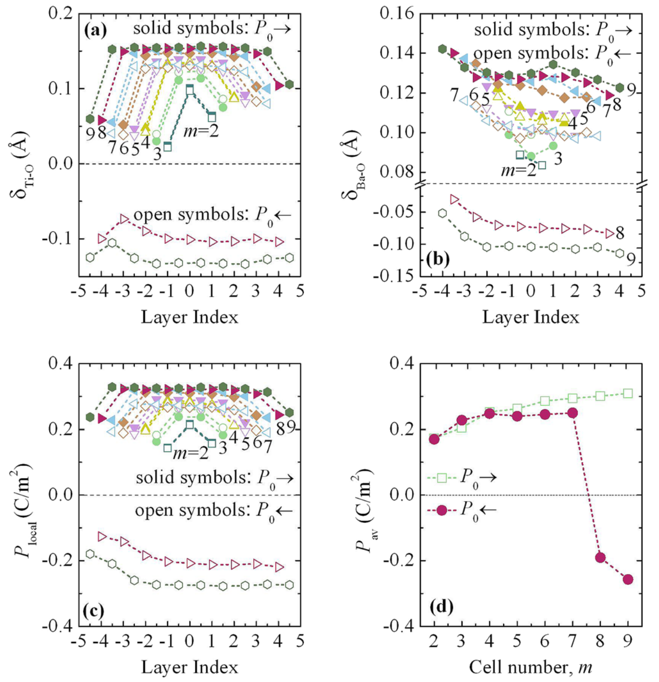

FIG. 9. Calculated results of Pt/(TiO_2-BaO)$_m$-TiO_2/SRO tunnel junctions with initial positive and negative ferroelectric distortions. (a) Ti-O rumpling of [001] TiO_2 monolayers. (b) Ba-O rumpling of [001] BaO monolayers. (c) Local polarization distribution. (d) Average polarization as a function of unit-cell number m. The layer index is set zero at the middle plane of the barrier.

atomic rumplings and local polarization near the specific interface (e.g., TiO_2/SrO or RuO_2/BaO interfaces) are found similar with those of the S-FTJs shown in Figs. 3(a) and 3(c). Interestingly, although the tunnel junctions have strong asymmetry, Fig. 9(c) shows that the local polarization distribution of the positive polarization state is quite symmetric. For this type of A-FTJs, the more stable polarization state is the positive polarization state (i.e., pointing from the Pt_2/TiO_2 to TiO_2/SrO interface), in consistence with the previous investigation in literature.[40] In particular, the negative polarization state is not stable in tunnel junctions with an initial negative ferroelectric distortion when their thickness is less than eight unit-cells. Moreover, the polarization gradually decreases as the barrier thickness decreases, and it maintains notable (i.e., $P_{av} \sim 017\,C/m^2$) when $m = 2$. Thus, there is absence of critical thickness for the positive polarization state. Similar with SRO/(BaO-TiO_2)$_m$/SRO tunnel junctions, we also found that the positive polarization state obtained in tunnel junctions with a negative ferroelectric distortion is not exactly the same with that obtained in tunnel junctions with an initial positive ferroelectric distortion, indicating complicated energy surface.

The calculated results of Pt/BaO-(TiO_2-BaO)$_m$/SRO tunnel junctions with initial positive and negative ferroelectric distortion are shown in Fig. 10. The local features of atomic rumplings and local polarization near the Pt_2/BaO and BaO/SRO interfaces are also found similar with those of the S-FTJs (see Figs. 3(b) and 3(d)). As a consequence of the distinct features of the two interfaces, the atomic rumplings and local polarization profiles are asymmetric and quite different for the two polarization state. For this type of A-FTJs, the more stable polarization state is the negative polarization state (i.e., pointing from BaO/RuO_2 to Pt_2/BaO interface), in contrary with Pt/(TiO_2-BaO)$_m$-TiO_2/SRO tunnel junctions shown in Fig. 9. The critical thickness of the positive polarization state is five unit-cells. The negative polarization state maintains a large magnitude ($P_{av} \sim 0.33\,C/m^2$) as the film thickness decreases. Compared with the result of Pt/(TiO_2-BaO)$_m$/Pt tunnel junctions, both the two types of tunnel junctions have more stable polarization state pointing into the Pt_2/BaO interface, indicating a dominant role of Pt_2/BaO interface in determining the polarization stability. It is also interesting to notice that the critical thickness of the less stable polarization state of this type of tunnel junctions is smaller than that of SRO/(BaO-TiO_2)$_m$/SRO tunnel junctions, although a large built-in field is found in the former type of tunnel junctions (see in the following). This may indicate a deeper valley of the energy surface of the former type of tunnel junctions.

In Fig. 11, we depict the calculated results of Pt/(BaO-TiO_2)$_m$/SRO tunnel junctions with initial positive and negative ferroelectric distortion. Similar with the other types of tunnel junctions involving Pt_2/BaO interface (see Figs. 3, 8, and 10), we found the relaxed structures have large Ba-O rumpling especially when the interfacial ferroelectric distortion is pointing away from the electrode, indicating again the well-kept local features of the specific interfaces in different types of tunnel junctions. As a result, the local polarization always has a larger magnitude at the Pt_2/BaO interface than at the other region. Moreover, compared with the results of Pt/BaO-(TiO_2-BaO)$_m$/SRO tunnel junctions as shown in Fig. 10, one can note that the atomic rumplings and local

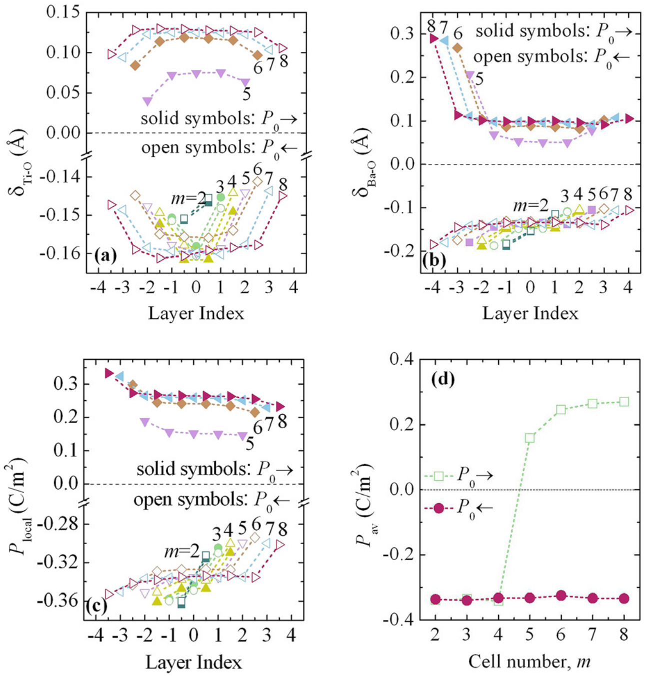

FIG. 10. Calculated results of Pt/BaO-(TiO_2-BaO)$_m$/SRO tunnel junctions with initial positive and negative ferroelectric distortions. (a) Ti-O rumpling of [001] TiO_2 monolayers. (b) Ba-O rumpling of [001] BaO monolayers. (c) Local polarization distribution. (d) Average polarization as a function of unit-cell number m. The layer index is set zero at the middle plane of the barrier.

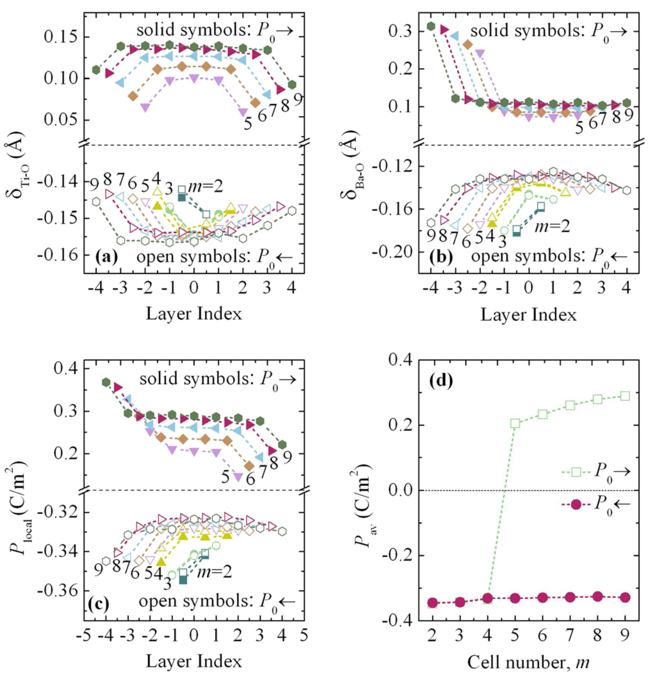

FIG. 11. Calculated results of Pt/(BaO-TiO_2)$_m$/SRO tunnel junctions with initial positive and negative ferroelectric distortions. (a) Ti-O rumpling of [001] TiO_2 monolayers. (b) Ba-O rumpling of [001] BaO monolayers. (c) Local polarization distribution. (d) Average polarization as a function of unit-cell number m. The layer index is set zero at the middle plane of the barrier.

polarization profiles are quite similar, except some difference at the right interfaces due to the different local features of TiO_2/SRO and BaO/SRO. This again provides evidence of the dominant role of Pt_2/BaO interface in determining the overall ferroelectric size effect of tunnel junctions. In agreement with the result of Luo *et al.*,[16] the critical thickness of positive polarization state in this type of tunnel junctions is about five unit-cells, below which it would flip into the negative polarization state. When decreasing barrier thickness, the average polarization of negative polarization state is slightly increased and reaches about $0.35\,C/m^2$ at $m = 2$, indicating an absence of critical thickness for this polarization state.

The calculated results of the last type of A-FTJs, i.e., Pt/(TiO_2-BaO)$_m$/SRO tunnel junctions, are shown in Fig. 12. It can be seen that the results are quite similar to those of Pt/(TiO_2-BaO)$_m$-TiO_2/SRO tunnel junctions, indicating the more dominant role of Pt_2/TiO_2 interface than the SRO/BTO interfaces in determining the performance of the tunnel junctions. The negative polarization state is not stable when thickness of BTO barrier is less than eight unit-cells. Moreover, the polarization gradually decreases as the barrier thickness decreases, and it maintains notable (i.e., $P_{\rm av} \sim 012\,C/m^2$) when $m = 2$, evidencing the absence of critical thickness for the positive polarization state. We also note that the positive polarization state obtained in tunnel junctions with a negative ferroelectric distortion is slightly different from that obtained in tunnel junctions with an initial positive ferroelectric distortion when $m = 5$, 6, and 7. Furthermore, it can be seen that the local polarization profile of this type of tunnel junctions is mainly in line with the Ti-O rumpling profile, as the Ba-O rumplings are in moderate magnitude.

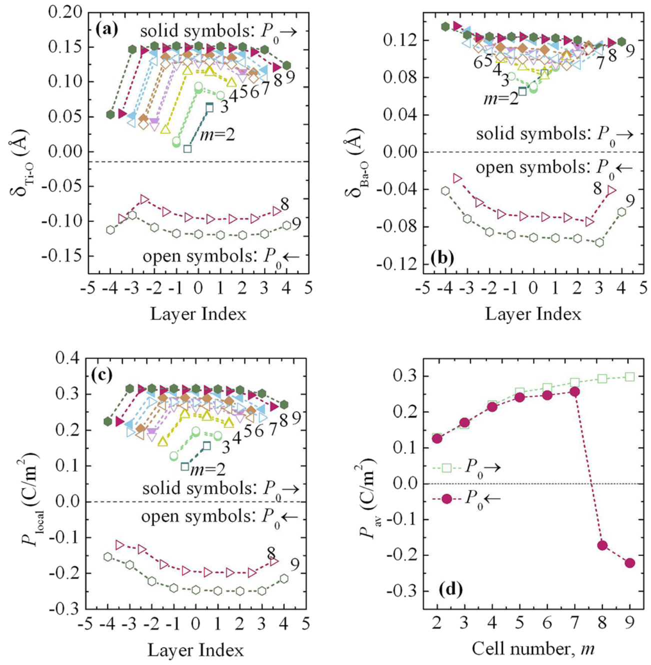

FIG. 12. Calculated results of Pt/(TiO_2-BaO)$_m$/SRO tunnel junctions with initial positive and negative ferroelectric distortions. (a) Ti-O rumpling of [001] TiO_2 monolayers. (b) Ba-O rumpling of [001] BaO monolayers. (c) Local polarization distribution. (d) Average polarization as a function of unit-cell number m. The layer index is set zero at the middle plane of the barrier.

To see the charge transfer at the interfaces of A-FTJs, we plotted the macroscopic-averaged differential electron charge density $\Delta\bar{\bar{\rho}}_{\rm scf\text{-}nscf}(z)$ for A-FTJs with $m = 8$ as shown in Fig. 13. Due to the asymmetry, both the positive and negative polarization states are calculated. From the results, it can be seen that the local feature of the charge transfer at specific interface is well kept in different types of tunnel junctions. Specifically, for all the tunnel junctions, there is an electron loss at the electrodes and an electron gain in the ferroelectric barrier, with larger charge transfer at the Pt/BTO interfaces than at the SRO/BTO interfaces. Comparison between the differential electron charge density at positive and the negative polarization states shows that the differential electron charge density would decrease (increase) at the left (right) interface as the tunnel junction changes from positive polarization state to negative polarization state, indicating the changed sign of surface polarization charge and screening charge at the interfaces. Similar with the S-FTJs, the coupling between electron transfer and the ferroelectric distortion at the SRO/BTO interfaces is found more sensitive than that at the Pt/BTO interfaces.

The calculated macroscopic-averaged electrostatic potential energy profile along z direction $\bar{\bar{V}}(z)$ of A-FTJs with $m = 8$ in positive and negative polarization states is

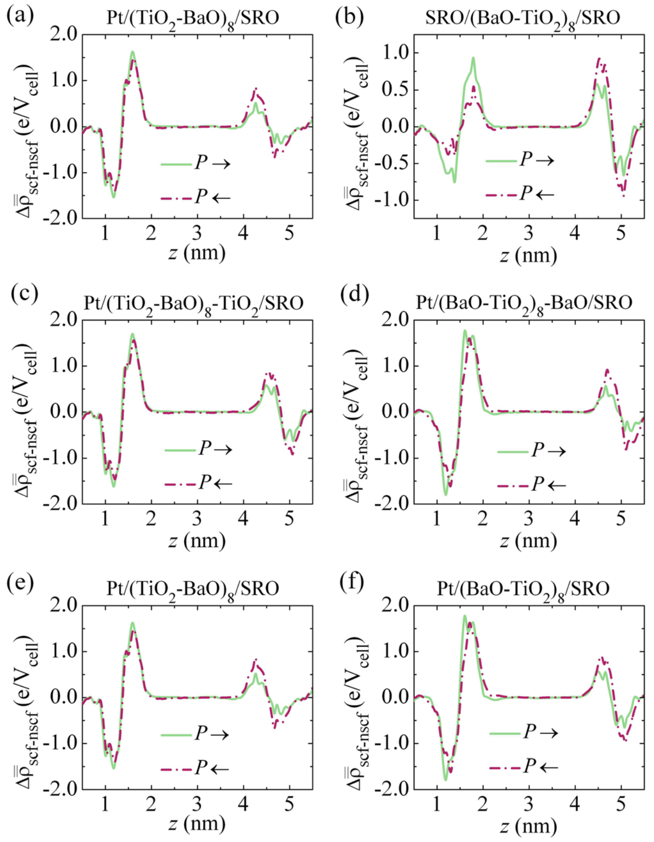

FIG. 13. Macroscopic-averaged differential charge density along z direction of A-FTJs in positive and negative polarization states. e is the charge of an electron and $V_{\rm cell}$ is the volume of the supercell. (a) Pt/(TiO_2-BaO)$_8$/Pt, (b) SRO/(BaO-TiO_2)$_8$/SRO, (c) Pt/(TiO_2-BaO)$_8$-TiO_2/SRO, (d) Pt/BaO-(TiO_2-BaO)$_8$/SRO, (e) Pt/(BaO-TiO_2)$_8$/SRO, and (f) Pt/(TiO_2-BaO)$_8$/SRO tunnel junction.

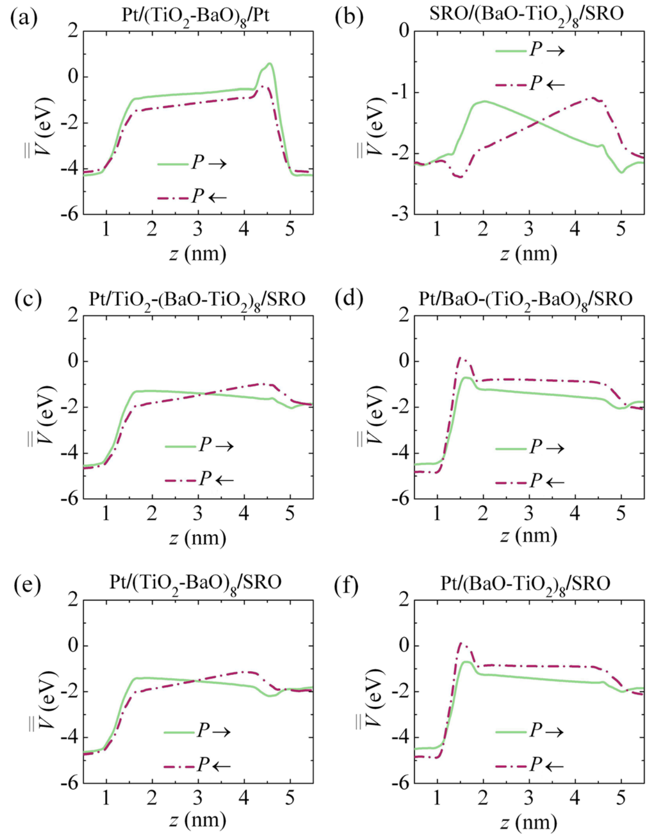

FIG. 14. Macroscopic-averaged electrostatic potential energy profile along z direction of A-FTJs in positive and negative polarization states. (a) Pt/(TiO$_2$-BaO)$_8$/Pt, (b) SRO/(BaO-TiO$_2$)$_8$/SRO, (c) Pt/(TiO$_2$-BaO)$_8$-TiO$_2$/SRO, (d) Pt/BaO-(TiO$_2$-BaO)$_8$/SRO, (e) Pt/(BaO-TiO$_2$)$_8$/SRO, and (f) Pt/(TiO$_2$-BaO)$_8$/SRO tunnel junction.

depicted Fig. 14. It can be seen that Pt/BTO interfaces have larger potential steps than SRO/BTO interfaces, as a consequence of the more significant interfacial charge transfer between the Pt electrode and barrier. Particularly, as shown in Fig. 14(a), the potential profiles of the two states in Pt/(TiO$_2$-BaO)$_8$/Pt tunnel junction have positive slopes, indicating the existence of a positive built-in field in the barrier. The magnitude of this built-in field can be roughly estimated as half of the sum of the electric field of the two states, which gives $E_b = \sim 1.95 \times 10^8$ V/m. This field is in the same direction of the positive polarization and thus has a strong polarizing effect on this state. One could also note that the average heights of the potential barrier of the two polarization states are different by quite an amount, which should have important effect on the electronic transport along the two directions. For SRO/(BaO-TiO$_2$)$_8$/SRO tunnel junction, the slopes of the potential profiles of the two states have different sign and are in the similar magnitude (see Fig. 14(b)). As a consequence, the average heights of the potential barrier in the two polarization state are similar. Actually, there is also a positive built-in field within the barrier of this tunnel junction, which is quite small ($\sim 2.7 \times 10^7$ V/m) compared with the other investigated A-FTJs. Nevertheless, as we have seen in the above, the small asymmetry of this type of tunnel junctions still leads to distinct size dependences of the two polarization states (see Fig. 8).

For A-FTJs with dissimilar electrodes, their potential energy profiles are expected to be more complicated. Indeed, from the potential profiles as shown in Figs. 14(c)–14(f), we can see that the potential has different levels inside the electrodes, with the average potential in the Pt electrode is about 2.7 eV lower than that in the SRO electrode. This value is almost the same with the estimated difference (~2.8 eV) of potential steps between Pt/BTO and SRO/BTO interfaces of S-FTJs in Sec. III B. For Pt/(TiO$_2$-BaO)$_8$-TiO$_2$/SRO tunnel junction (see Fig. 14(c)), while the potential slope changes its sign for the two polarization state, the total electric field within the barrier is much larger in the negative polarization state. Actually, a positive built-in field ($\sim 0.9 \times 10^8$ V/m) exists in the barrier, which makes the negative polarization state metastable. Interestingly, comparing with the result of Pt/(TiO$_2$-BaO)$_8$/Pt tunnel junction in Fig. 14(a), we can see that adopting dissimilar electrodes in the A-FTJ does not necessary lead to a larger built-in field. The potential profiles of Pt/BaO-(TiO$_2$-BaO)$_8$/SRO tunnel junction and Pt/(TiO$_2$-BaO)$_8$/SRO tunnel junction as, respectively, shown in Figs. 14(d) and 14(f) are found similar with that of Pt/(TiO$_2$-BaO)$_8$/Pt tunnel junction, with a large built-in field pointing to the Pt/BTO interface, indicating the dominant role of Pt/BTO interface in determining the potential profile of the tunnel junctions.

C. A comprehensive picture of size effect on ferroelectricity of FTJs as a function of electrode/ferroelectric interfaces

The presented results clearly show that the details of the two interfaces have great impacts on the ferroelectric size effect of FTJs. The thickness dependence of the average polarization for all the investigated S-FTJs and A-FTJs has been re-plotted in Fig. 15, which provides us a comprehensive picture of the ferroelectric size effect as a function of electrode/ferroelectric interfaces. Obviously, with adjusting the electrodes and interfacial bondings of FTJ, fruitful ferroelectric size effects can be exhibited.

Summarizing the results of investigated electrostatic properties of FTJs, e.g., interfacial charge transferring and potential profiles, we can also see that these properties depend on the details of the interfaces, which cannot simply obtained by knowing the bulk properties of electrodes and ferroelectrics. Particularly, for A-FTJs with the same combination of top and bottom electrodes, their built-in field can be significantly different in magnitude and even in sign due to the different interfacial bondings, indicating that the conventional electrostatic model which assumes that the built-in field originates from the work function difference between the bulk electrodes is not plausible.[57] Instead, the built-in field should be calculated by the work functions at the two interfaces, which are strongly dependent on the interfacial structures.[31,37]

Therefore, it is necessary to explore ferroelectricity-related properties of FTJs with regard to the details of interfaces. In general, to quantitatively reproduce the size effect of FTJs, the short-range and long-range features of specific interfaces and of their combination should be appropriately

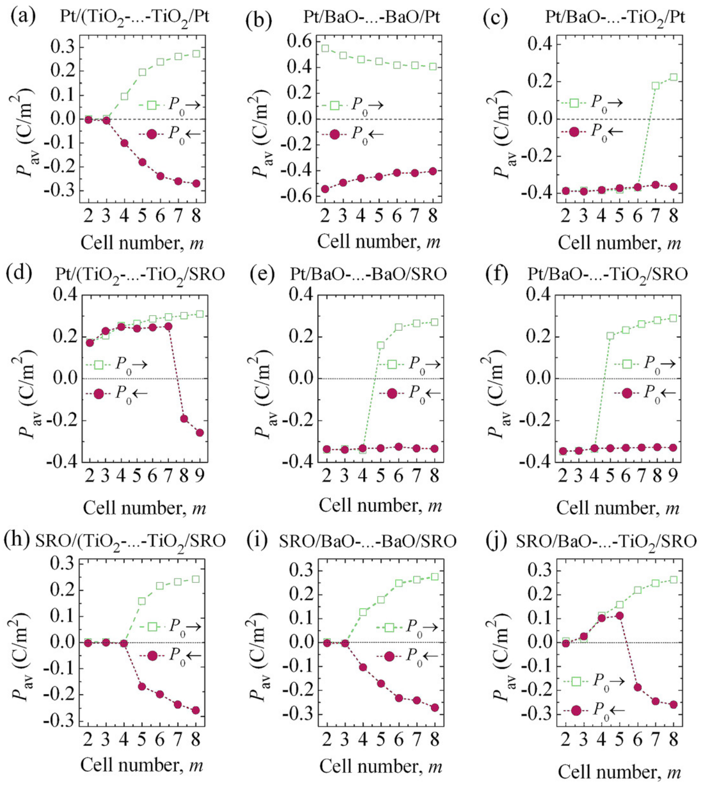

FIG. 15. The thickness dependence of the average polarization for all the investigated S-FTJs and A-FTJs. (a) Pt/(TiO_2-BaO)$_m$-TiO_2/Pt, (b) Pt/BaO-(TiO_2-BaO)$_m$/Pt, (c) Pt/(BaO-TiO_2)$_m$/Pt, (d) Pt/(TiO_2-BaO)$_m$-TiO_2/SRO, (e) Pt/BaO-(TiO_2-BaO)$_m$/SRO, (f) Pt/(BaO-TiO_2)$_m$/SRO, (g) Pt/(TiO_2-BaO)$_m$/SRO, (h) SRO/(TiO_2-BaO)$_m$-TiO_2/SRO, (i) SRO/BaO-(TiO_2-BaO)$_m$/SRO, and (j) SRO/(BaO-TiO_2)$_m$/SRO tunnel junctions.

taken into account. These features include the interfacial structure, local polarization, charge transfer, potential step, electronic screening, polarizing/built-in fields, etc. With regard to this issue, several modified phenomenological models have been proposed in literature,[35,37,38,41,42,45] nevertheless, at present a comprehensive model that incorporates well both the short- and long-range features of the interfaces is still lacking.

Importantly, the interfacial structures are found coupled with the polarization state of the barrier. Through this coupling, strong polarizing/built-in field may appear and enhancement of polarization in FTJs is possible, as clearly seen in tunnel junctions with Pt/BaO interface. In order to quantitatively reproduce the size effect of FTJs, this coupling effect should be also taken into account in traditional phenomenological model, e.g., by introducing new order parameters to represent the change of interfacial structures.[37] Accordingly, the dynamics of polarization should be solved in conjunction with the evolution of interfacial structure. As a result, the aforementioned short- and long-range features of the interfaces are likely to be varied during dynamics of polarization, thus cannot be regarded as constants. It would be also worth to point out that interfacial structure should be sensitive to the strain state of the tunnel junction. Novel strain-controlling ferroelectric size effects may hide behind the coupling between the interfacial structures and strains and should be interesting to investigate.

The distinct features of A-FTJs from its symmetric counterparts should have important implications on the application of A-FTJs, which is also an interesting topic for future investigation. Actually, the existence of a less stable polarization state means that below a specific thickness, the tunnel junction would lose polarization bistability. A critical thickness of polarization bistability could pose limitation on applications of A-FTJs based on polarization reversal, such as the GER effect[43] and GPR effect.[45] Nevertheless, we believe that the asymmetry-induced features of A-FTJs (e.g., asymmetric polarization states, critical thickness of bistability, and the related built-in field) could bring additional effects, which can be exploited for prospective applications. Indeed, by making use of the built-in field of A-FTJs, effects like smearing of the phase transition, induced piezoelectric response above transition temperature, and reversal of the polarization asymmetry by application of biaxial strain have been predicted.[38,42]

IV. CONCLUSIONS

In summary, we have conducted first-principle calculations to systematically investigate the ferroelectric size effect of BTO tunnel junctions with metal Pt and/or oxide SRO electrodes. Fully relaxations of the supercells are achieved via including a vacuum region in the supercell calculations. The characteristics of atomic structure, polarization, charge density, and electrostatic potential for ten possible types of tunnel junctions are revealed. Significant dependence of the ferroelectric stability of a tunnel junction on the type and combination of the two interfaces has been demonstrated. Results show that the Pt/BTO interfaces play more dominant roles than SRO/BTO in affecting the ferroelectric stability of the tunnel junctions. Particularly, it is found that Pt_2/TiO_2 interface can induce collective ferroelectric distortion in the initially non-distorted barrier. An abnormal enhancement of ferroelectricity by Pt_2/BaO interface due to Pt-O bonding effect is also demonstrated. For asymmetric tunnel junctions, polarization stability is found dependent on direction, manifested with the appearing of a critical thickness of polarization bistability. Furthermore, result shows that the local features of a specific electrode/ferroelectric interface (e.g., the interfacial atomic structure, local polarization, charge transfer, and potential step) are well kept in different types of tunnel junctions. By analyzing and summarizing the results, the authors suggest that traditional phenomenological models need several modifications in order to quantitatively reproduce the size effect of ferroelectric tunnel junctions.

ACKNOWLEDGMENTS

Helpful discussions with G. H. Zhang and H. F. Li are gratefully acknowledged. The authors also gratefully acknowledge the financial support of NSFC (Nos. 10902128, 10732100, 50802026, 10972239). Y. Zheng also thanks support by the Fundamental Research Funds for the Central Universities, NCET in University, Research Fund for the Doctoral Program of Higher Education, and Fok Ying Tung Foundation, Science and Technology Innovation Project of Guangdong Provincial Education Department and Guangdong Natural Science Funds for Distinguished Young Scholar.

[1] M. E. Lines and A. M. Glass, *Principles and Applications of Ferroelectrics and Related Materials* (Clarendon, Oxford, 1977).
[2] D. Damjanovic, Ferroelectric. Rep. Prog. Phys. **61**, 1267 (1998).
[3] *Physics of Ferroelectrics: A Modern Perspective*, edited by K. M. Rabe, C. H. Ahn, and J.-M. Triscone (Springer, Berlin, 2007).
[4] J. F. Scott, Science **315**, 954 (2007).
[5] C. H. Ahn, K. M. Rabe, and J.-M. Triscone, Science **303**, 488 (2004).
[6] J. F. Scott, J. Phys.: Condens. Matter **18**, R361 (2006).
[7] J. F. Scott, F. D. Morrison, M. Miyake, and P. Zubko, Ferroelectrics **336**, 237 (2006).
[8] A. Gruverman and A. Kholkin, Rep. Prog. Phys. **69**, 2443 (2006).
[9] P. M. Rørvik, T. Grande, and M.-A. Einarsrud, Adv. Mater. **23**, 4007 (2011).
[10] A. N. Morozovska, E. A. Eliseev, and M. D. Glinchuk, Phys. Rev. B **73**, 214106 (2006).
[11] Y. Zheng, C. H. Woo, and B. Wang, J. Phys.: Condens. Matter **20**, 135216 (2008).
[12] M. S. Majdoub, P. Sharma, and T. Cagin, Phys. Rev. B **77**, 125424 (2008).
[13] M. J. Highland, T. T. Fister, M.-I. Richard, D. D. Fong, P. H. Fuoss, C. Thompson, J. A. Eastman, S. K. Stephen, and G. B. Stephenson, Phys. Rev. Lett. **105**, 167601 (2010).
[14] A. N. Morozovska, E. A. Eliseev, M. D. Glinchuk, and R. Blinc, Phys. Rev. B **81**, 092101 (2010).
[15] Y. Zheng, S. P. Lin, and B. Wang, Appl. Phys. Lett. **99**, 062904 (2011).
[16] X. Luo, Y. Zheng, and B. Wang, J. Appl. Phys. **111**, 074102 (2012).
[17] W. J. Chen, Y. Zheng, and B. Wang, Sci. Rep. **2**, 796 (2012).
[18] R. R. Mehta, B. D. Siilverman, and J. T. Jacobs, J. Appl. Phys. **44**, 3379 (1973).
[19] I. P. Batra, P. Wurfel, and B. D. Silverman, Phys. Rev. B **8**, 3257 (1973).
[20] R. Kretschmer and K. Binder, Phys. Rev. B **20**, 1065 (1979).
[21] I. I. Naumov, L. Bellaiche, and H. Fu, Nature (London) **432**, 737 (2004).
[22] A. Schilling, R. M. Bowman, G. Catalan, J. F. Scott, and J. M. Gregg, Nano Lett. **7**, 3787 (2007).
[23] L. Louis, P. Gemeiner, I. Ponomareva, L. Bellaiche, G. Geneste, W. Ma, N. Setter, and B. Dkhil, Nano Lett. **10**, 1177 (2010).
[24] M. J. Polking, M.-G. Han, A. Yourdkhani, V. Petkov, C. F. Kisielowski, V. V. Volkov, Y. Zhu, G. Caruntu, A. P. Alivisatos, and R. Ramesh, Nature Mater. **11**, 700 (2012).
[25] T. Tybell, C. H. Ahn, and J. M. Triscone, Appl. Phys. Lett. **75**, 856 (1999).
[26] D. D. Fong, G. B. Stephenson, S. K. Streiffer, J. A. Eastman, O. Auciello, P. H. Fuoss, and C. Thompson, Science **304**, 1650 (2004).
[27] D. D. Fong, A. M. Kolpak, J. A. Eastman, S. K. Streiffer, P. H. Fuoss, G. B. Stephenson, C. Thompson, D. M. Kim, K. J. Choi, C. B. Eom, I. Grinberg, and A. M. Rappe, Phys. Rev. Lett. **96**, 127601 (2006).
[28] D. A. Tenne, A. Bruchhausen, N. D. Lanzillotti-Kimura, A. Fainstein, R. S. Katiyar, A. Cantarero, A. Soukiassian, V. Vaithyanathan, J. H. Haeni, W. Tian, D. G. Schlom, K. J. Choi, D. M. Kim, C. B. Eom, H. P. Sun, X. Q. Pan, Y. L. Li, L. Q. Chen, Q. X. Jia, S. M. Nakhmanson, K. M. Rabe, and X. X. Xi, Science **313**, 1614 (2006).
[29] D. A. Tenne, P. Turner, J. D. Schmidt, M. Biegalski, Y. L. Li, L. Q. Chen, A. Soukiassian, S. Trolier-McKinstry, D. G. Schlom, X. X. Xi, D. D. Fong, P. H. Fuoss, J. A. Eastman, G. B. Stephenson, C. Thompson, and S. K. Streiffer, Phys. Rev. Lett. **103**, 177601 (2009).
[30] J. Junquera and P. Ghosez, Nature (London) **422**, 506 (2003).
[31] N. Sai, A. M. Kolpak, and A. M. Rappe, Phys. Rev. B **72**, 020101(R) (2005).
[32] C.-G. Duan, R. F. Sabirianov, W.-N. Mei, S. S. Jaswal, and E. Y. Tsymbal, Nano Lett. **6**, 483 (2006).
[33] M. Sepliarsky, M. G. Stachiotti, and R. L. Migoni, Phys. Rev. Lett. **96**, 137603 (2006).
[34] G. Gerra, A. K. Tagantsev, N. Setter, and K. Parlinski, Phys. Rev. Lett. **96**, 107603 (2006).
[35] A. K. Tagantsev, G. Gerra, and N. Setter, Phys. Rev. B **77**, 174111 (2008).
[36] M. Stengel, D. Vanderbilt, and N. A. Spaldin, Nature Mater. **8**, 392 (2009).
[37] M. A. M. Polanco, I. Grinberg, A. M. Kolpak, S. V. Levchenko, C. Pynn, and A. M. Rappe, Phys. Rev. B **85**, 214107 (2012).
[38] G. Gerra, A. K. Tagantsev, and N. Setter, Phys. Rev. Lett. **98**, 207601 (2007).
[39] Y. Umeno, J. M. Albina, B. Meyer, and C. Elsässer, Phys. Rev. B **80**, 205122 (2009).
[40] M.-Q. Cai, Y. Zheng, P.-W. Ma, and C. H. Woo, J. Appl. Phys. **109**, 024103 (2011).
[41] G. B. Stephenson and M. J. Highland, Phys. Rev. B **84**, 064107 (2011).
[42] Y. Zheng, W. J. Chen, X. Luo, B. Wang, and C. H. Woo, Acta Mater. **60**, 1857 (2012).
[43] M. Y. Zhuravlev, R. F. Sabirianov, S. S. Jaswal, and E. Y. Tsymbal, Phys. Rev. Lett. **94**, 246802 (2005).
[44] A. Gruverman, D. Wu, H. Lu, Y. Wang, H. W. Jang, C. M. Folkman, M. Ye. Zhuravlev, D. Felker, M. Rzchowski, C.-B. Eom, and E. Y. Tsymbal, Nano Lett. **9**, 3539 (2009).
[45] Y. Zheng and C. H. Woo, Nanotechnology **20**, 075401 (2009).
[46] D. Pantel and M. Alexe, Phys. Rev. B **82**, 134105 (2010).
[47] J. P. Velev, C.-G. Duan, K. D. Belashchenko, S. S. Jaswal, and E. Y. Tsymbal, Phys. Rev. Lett. **98**, 137201 (2007).
[48] X. Luo, Y. Zheng, and B. Wang, ACS Nano **5**, 1649 (2011).
[49] G. Kresse and J. Furthmüller, Phys. Rev. B **54**, 11169 (1996).
[50] P. E. Blöchl, Phys. Rev. B **50**, 17953 (1994).
[51] J. P. Perdew and A. Zunger, Phys. Rev. B **23**, 5048 (1981).
[52] H. J. Monkhorst and J. D. Pack, Phys. Rev. B **13**, 5188 (1976).
[53] A. M. Kolpak, N. Sai, and A. M. Rappe, Phys. Rev. B **74**, 054112 (2006).
[54] R. D. King-Smith and D. Vanderbilt, Phys. Rev. B **47**, 1651 (1993).
[55] A. Baldereschi, S. Baroni, and R. Resta, Phys. Rev. Lett. **61**, 734 (1988).
[56] J. Junquera, M. H. Cohen, and K. M. Rabe, J. Phys.: Condens. Matter **19**, 213203 (2007).
[57] J. G. Simmons, Phys. Rev. Lett. **10**, 10 (1963).